ACS APPLIED MATERIALS & INTERFACES

Research Article

www.acsami.org

Synthesis of Au-Decorated Tripod-Shaped Te Hybrids for Applications in the Ultrasensitive Detection of Arsenic

Demeng Wang,[†] Yuewu Zhao,[†] Huile Jin,[†] Jinxia Zhuang,[†] Weiming Zhang,[†] Shun Wang,*[,†,‡] and Jichang Wang*[,†,§]

[†]Nano-materials & Chemistry Key Laboratory, Wenzhou University, Wenzhou, Zhejiang, China 325035

[‡]State Key Lab of Silicon Materials, Zhejiang University, Hangzhou, China 310027

[§]Department of Chemistry and Biochemistry, University of Windsor, Ontario, Canada N9B 3P4

Supporting Information

ABSTRACT: Novel Au-decorated Te hybrids with a tripod-shaped planar microstructure were prepared through a two-step hydrothermal process: the synthesis of Te single crystals and the subsequent self-sacrificial reaction of Te template with $HAuCl_4$. Based on the influences of reaction temperature and solvent compositions on the as-obtained microstructures, a plausible mechanism was proposed to account for the formation of the tripod-shaped Te and Au/Te crystals. The as-prepared Au/Te hybrids have the sensitivity of 6.35 μA/ppb in the electrochemical detection of As(III), which represents the highest sensitivity reported in literature. The Au/Te sensor also has a low detection limit of 0.0026 ppb and could work in complex mixtures containing As(III), Cu(II) and other heavy metal ions, exhibiting excellent selectivity on As(III) and Cu(II) ions. The enhanced electrocatalytic property may be attributed to the synergetic interactions between the noble metal and semiconductor and the presence of a large number of active sites on the hybrids surface.

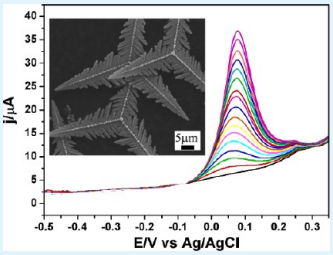

KEYWORDS: *Au/Te hybrids, electrochemical analysis, arsenic ions, hydrothermal synthesis, heavy metal ions*

1. INTRODUCTION

The highly toxic arsenic is widely distributed in nature and the contamination of water by arsenic is a major problem in many countries.[1−4] Being able to detect trace amount of arsenic in contaminated water is needed to avoid their accumulation to a level that imposes great threat on public health.[4] Among the methods that have been developed for the sensitive detection and quantification of arsenic, the low-cost electrochemical techniques such as stripping voltammetry have attracted significant interest because of their portability and suitability for on-site analysis.[5]

For the electrochemical determination of arsenic various solid electrodes have been developed, yet Au has shown by far the most promising properties in the sensitive detection of arsenic (see Table 1 for the summary).[6−19] For example, Ohsaka's group used the Au(111)-like poly-Au electrode to obtain the sensitive detection of As(III) without any interference from Cu(II).[6] Recent progress in the study of nanomaterials offers a new route to further improve the sensitivity of Au in arsenic detection. Gold nanoparticles modified glassy carbon electrode developed by Compton and co-workers achieved a detection limit of 0.0096 ppb in the voltammetric determination of arsenic.[7]

It has lately become well-known that properties of nanomaterials are strongly influenced by their dimensionality and shape.[20−25] Extensive efforts have recently been devoted to the synthesis of different micro/nano crystals in the attempt of achieving new or better applications of existing materials. As a result, various crystallines with different morphologies such as nanowires,[26−28] nanorods,[29,30] nanotubes,[31,32] and nanobelts[33−35] have been reported. In comparison to one-dimensional (1D) nanomaterials, shape-controlled synthesis of three-dimensional (3D) complex architectures still represents a great challenge in materials science,[36] despite the fact that 3D configurations may lead to new physical and chemical properties.[37−39]

To explore applications of 3D nanomaterials and benefit from synergetic interactions of noble metal hybrids, in this study, we developed a hydrothermal approach to prepare 3D Au/Te hybrid crystalline. This new process does not require the assistance of seeding or surfactants. The selection of Te is motivated by the fact that it has already been used in various areas such as piezoelectronic devices, photoconductive detectors, thermoelectronic and gas-sensing materials,[40−42] and has also been employed to prepare hybrid materials with a desired morphology.[43,44] Notably, because of their highly anisotropic property Te atoms normally form unique helical chain structure and 3D nanostructures have been proved to be much difficult to synthesize.[45−48]

In this study, Au decorated tripod-shaped Te crystallines were synthesized by using diethyldithiocarbamato tellurium(IV) (TDEC) as the Te source and 2, 2′-dithiodibenzoic acid (DTBA) as the organic reducing reagent. The addition of ethanol as a cosolvent was found to be critical in obtaining the uniform tripod-shaped crystallines. Employing square wave anodic stripping

Received: April 2, 2013
Accepted: June 3, 2013
Published: June 3, 2013

   dx.doi.org/10.1021/am401205w | ACS Appl. Mater. Interfaces 2013, 5, 5733−5740

Table 1. Summary of the Performance of Electrochemical Sensors Developed for the Detection of As(III)[a]

electrodes	electrolyte	linearity range (ppb)	sensitivity (μa/ppb)	LOD (ppb)	ref
Au NPs/GC	1 M HCl	0−7.5	0.24	0.0096	6
Au(111)-like Au electrode	PBS (pH = 1)	0−1125	0.3636	0.28	7
Au-UMEA	2 M HCl	0−500	0.044	0.013	8
Au NPs/GC	3 M HCl	0−87	4.27	1.8	9
Sonically assisted Au microdisk electrode	0.1 M HNO_3	7.5−75	0.363	0.2775	10
Au-coated diamond thin-film electrode	1 M HCl	0.01−40	0.0097	0.005	11
Au nanoelectrode ensembles	1 M HCl	0.1−3	3.14	0.02	12
Au-carbon composite electrode	0.1 M HNO_3	1.5−16.5	0.133	0.375	13
MWCNTs/Au electrode	acetic buffer (pH 4)		0.236		14
IrOx/BDD	PBS (pH 4.3)	1.5−3750	0.056	0.15	15
PBSPE	KCl/HCl (pH 4)	3.75−22500	3.87×10^{-4}	1.875	16
MWCNTs/Aro/GC	PBS (pH 7)	0−500	0.00143	1.0	17
CoOx/GC	PBS (pH 7)	15−300	0.00148	0.825	18
Fe_3O_4-RTIL/SPCE	acetic buffer (pH 5)	1−10	4.91	0.0008	19
Au-decorated Te hybrid electrode	1 M HCl	0.1−10	6.35	0.0026	This work

[a]Au NPs, gold nanoparticles; GC, glassy carbon electrode; Au-UMEA, gold ultramicroelectrode array; MWCNTs, multiwalled carbon nanotubes; IrOx, iridium oxide; BDD, boron-doped diamond; PBSPE, prussian blue-modified screen-printed electrode; Aro, arsenite oxidase; CoOx, cobalt oxide; RTIL, room temperature ionic liquid; SPCE, screen printed carbon electrode; PBS, phosphate buffer solution.

voltammetry (SWASV) the Au/Te hybrid electrode was able to simultaneously detect As(III) and Cu(II), in which two well-isolated anodic peaks separated by more than 100 mV were obtained. The detection limit of As(III) is 0.0026 ppb (S/N = 3) accompanied by a high sensitivity of 6.35 μA/ppb.

2. EXPERIMENTAL SECTION

2.1. The synthesis of Te and Au-Decorated Te Crystallines. Commercial grade diethyldithiocarbamato tellurium(IV) (TDEC) (from Zhejiang Ultrafine Powders & Chemicals Co. Ltd., P. R. China) was recrystallized twice from high-purity chloroform prior to its usage. Analytical grade 2,2′-dithiodibenzoic acid (DTBA), chloroform and absolute ethanol were purchased from Aldrich. Deionized water was prepared from a Milli-Q system (18.2 MΩ). In a typical procedure, 0.195 mmol of TDEC was dissolved in 10.0 mL of $CHCl_3$ in a 50 mL Teflon-lined stainless-steel autoclave to form a homogeneous solution. Then 0.65 mmol of DTBA and 15.0 mL of absolute ethanol were added to the autoclave. The autoclave was sealed and maintained at 130 °C for 5 h, and then naturally cooled to room temperature. Black solids formed at the bottom of the autoclave were collected and washed several times with deionized water and absolute ethanol and then dried in vacuum at room temperature for 12 h.

Au-decorated Te hybrids were synthesized as follows: 0.05 mM of the as-synthesized Te crystals and 0.1 mM of $HAuCl_4$ were added to a 20.0 mL glycol solution under continuous stirring. The above mixture was kept at 60 °C for 4 h. After that, the solid products were collected from the solution by centrifugation. The precipitates were washed several times with deionized water and absolute ethanol and were dried in a vacuum at room temperature for 12 h.

2.2. Apparatus. The as-prepared samples were characterized by X-ray diffraction (XRD) on a Bruker D8 Advance diffractometer using Cu Kα radiation (λ= 0.15406 nm). The data was collected in the 2θ range of 20−80° at a step size of 0.02°. The morphology was observed by scanning electron microscopy (SEM) on a FEI Nova Nanosem 200 microscope operated at an acceleration voltage of 10−15 kV. The transmission electron microscopy (TEM) images, high-resolution transmission electron microscopy (HRTEM) image and energy dispersive X-ray spectrometry (EDS) were taken on a JEOL 2010 high-resolution transmission electron microscope performed at 200 kV. Square wave anodic stripping voltammetry experiments were performed with a CHI760d electrochemical analyzer (CH Instruments, Chenhua Co., China).

2.3. Electrochemical Detection of As(III) and Other Heavy Metal Ions. To prepare the working electrode, about 5.0 mg of the as-prepared Au/Te hybrids was ultrasonically suspended in a mixture of 2.0 mL of ethanol and 50 uL of 5 wt % Nafion solution for about 5 min to obtain an ink. Twenty microliters of the ink was then spread on the surface of a glass carbon electrode. Reagents As_2O_3 (99.995%), $Pb(NO_3)$ (99.998%), $CuSO_4{\cdot}5H_2O$ (99.999%), $CrCl_3{\cdot}6H_2O$(99.99%), $FeCl_3{\cdot}6H_2O$(99.98%), $CdCl_2{\cdot}2H_2O$(99.99%), $NiCl_2{\cdot}6H_2O$(99.99%), $HgCl_2$(99.998%), $ZnCl_2$(99.99%), and $Mn(NO_3)_2$(99.99%) were obtained from Aldrich and were used as received. A stock solution (1 g/L) of As(III) was prepared by dissolving the required quantity of As_2O_3 in NaOH solution, and subsequently the pH of the solution was adjusted to 3 with concentrated HCl. (***Caution!*** *As_2O_3 and $HgCl_2$ are highly toxic; proper care must be taken in handling.*)

Square wave anodic stripping voltammetry (SWASV) was used for the detection of arsenic under optimized conditions. The bare Au electrode that is used in control experiments has a diameter of 2.0 mm (purchased from CHI Shanghai). A conventional three-electrode cell was used, with saturated Ag/AgCl as the reference electrode, a platinum wire as the counter electrode, and Au/Te-modified glassy carbon electrode as the working electrode. Arsenic was deposited at the potential of −0.30 V for 120 s by the reduction of As(III) in 1.0 M HCl. The anodic stripping (i.e., the oxidation of the deposited As(0)) was performed in the potential range of −0.50 to 0.5 V (vs Ag/AgCl electrode) at the following optimized parameters: frequency = 80 Hz, amplitude = 20 mV, and potential increment = 4 mV. The simultaneous and selective detection of As(III) and Cu(II) were performed at the same experimental condition as listed above.

3. RESULTS AND DISCUSSION

Figure 1 displays SEM, TEM, and HRTEM images of the as-synthesized Te products. The low-magnification SEM image in Figure 1a shows that the Te products consist of uniform planar tripod-shaped crystal. From the high-magnification SEM image in Figure 1b, it is clear that all three main branches of the superstructure are made up by many sharp secondary branches. The length of these main branches ranges from 25 to 35 μm. Those secondary branches are parallel to each other, whereas their length decreases as it moves toward the tip of those main branches. Images c and e in Figure 1 are TEM images recorded at the secondary and main branches of the Te crystal and their corresponding HRTEM images are presented in images d and f in Figure 1. The interplanar spacing is the same in both cases. The measured value of 0.385 nm is very close to the spacing of (100) plane of hexagonal-phase Te, suggesting that the crystal grew preferentially along the [100] direction. The fact that the

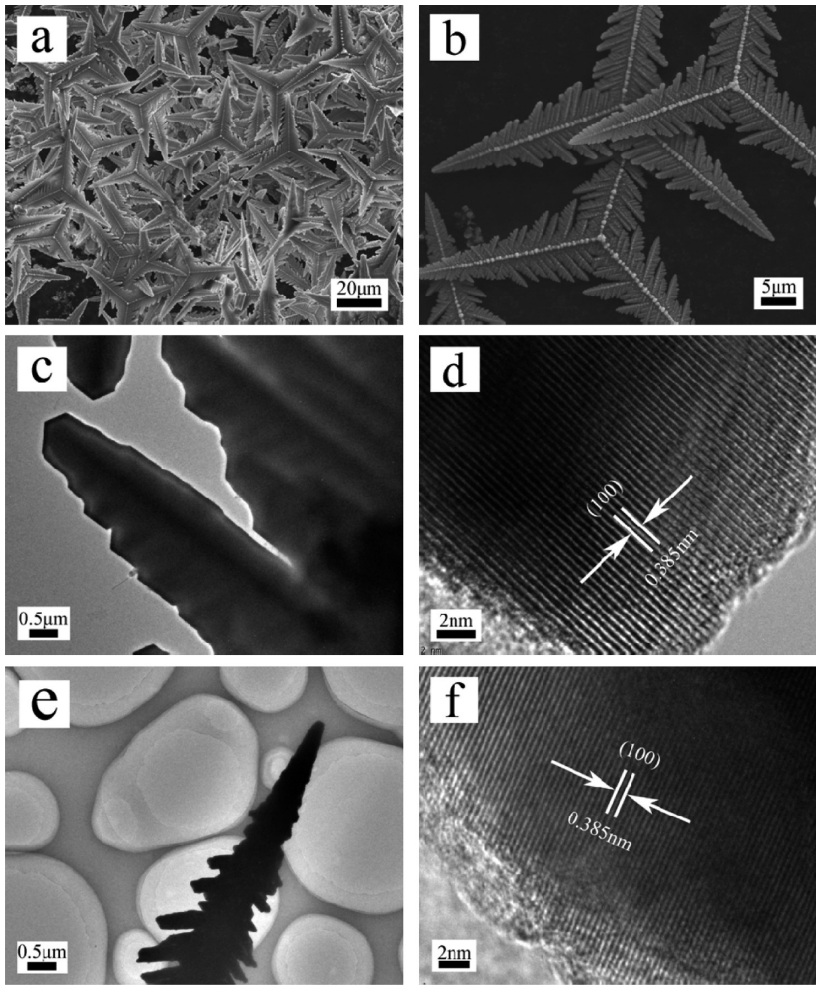

Figure 1. (a) Low-magnification SEM image, (b) high-magnification SEM, (c) TEM, (d) HRTEM, (e) TEM, and (f) HRTEM. Images a, b, e, and f were taken from the main branch, whereas c and d were images of the secondary branch of the Te products.

same interplanar spacing was obtained with the main and the secondary branches also suggests that the individual tripod-shaped Te crystal is a single-crystal with an identical orientation.

XRD spectroscopy of the above Te products was also measured (see Figure S1 in the Supporting Information), where all the peaks in the XRD pattern could be indexed to a pure hexagonal phase Te (cell constants a = 0.4458 nm, c = 0.5927 nm; JCPDS Card No. 36−1452). There is no impurity peaks detected, indicating that the sample is a high purity product. The sharp and strong diffraction peaks reveal that the Te products are well-crystallized. The energy-dispersive X-ray spectroscopy (EDS) further confirms that the as-prepared products are pure Te (see Figure S2 in the Supporting Information).

To gain insights into the development of the above tripod-shaped superstructure, we analyzed Te products at different reaction stages. Figure 2 shows the microstructures of Te products collected at (a, b) 3, (c, d) 4, (e, f) 4.5, (g, h) 5, and (i, j) 6 h after the start of the reaction. Images a and b in Figure 2 indicate that when the reaction time is 3 h, the main products are Te nanoparticles. As the reaction time is increased to 4 h, the reaction products become a mixture of a small quantity of nanoparticles and a large amount of three-bladed flakes. The length of each blade is about 10 μm (Figure 2c, d). Prolonging the reaction time further to 4.5 h, each blade grows longer to near 15 μm (Figure 2e, f). If the reaction is allowed to continue for a longer period of time such as 5 h, the length of the main branch increases to 25−35 μm (Figure 2g, h). For a reaction time of 6.0 h, the size and morphology of these well-defined tripod-shaped crystals remains the same (Figure 2i,j). Notably, all of the above products are hexagonal-phase Te crystalline.

On the basis of the SEM measurements in Figure 2, the formation of Te tripod superstructures can be loosely described as the following: Within the first 3 h, Te elements were produced through the reaction of TDEC and DTBA and aggregated to form nanosized nuclei for the subsequent crystal growth. The formation of Te nanoparticles within the first 3 h is mainly driven by the fact that smaller particles have larger surface energy. To achieve the surface-energy minimization, those small Te nanoparticles aggregated/grew into large crystals.[49] From there, further growth of the crystal is determined by two factors: (1) reaction kinetics (i.e., the rate of element Te formation), and (2) thermodynamics (i.e., facet energy). Although Te crystals have the tendency to grow along a certain direction due to their intrinsic anisotropic property, here Te clusters grew along three directions that were apart by 120 degree. Such a directional growth shall be contributed to the possible interactions between the solvent and a particular facet of the Te crystal. After all, the achievement of this distinct planar tripod structure in the absence of any seeding and surfactant shall be contributed to the influences of thermodynamic and reaction kinetics.

The influence of reaction temperature on the morphology of Te crystals was also characterized in this research. From the SEM

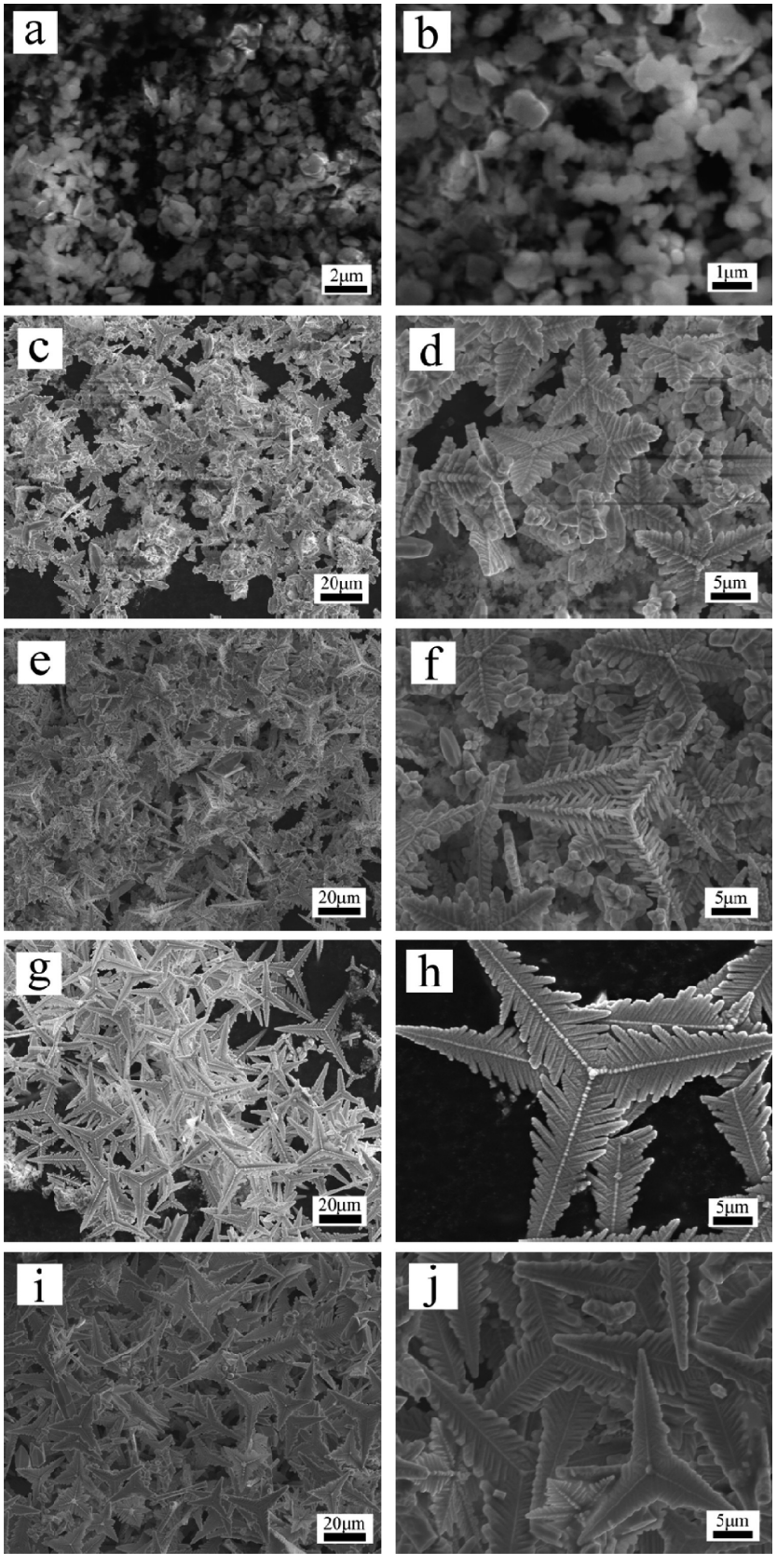

Figure 2. SEM images of Te produced at different reaction times: (a, b) 3, (c, d) 4, (e, f) 4.5, (g, h) 5, and (i, j) 6 h. The reaction temperature was 130 °C.

images (see Figure S3 in the Supporting Information), one can find that at the reaction temperature of 110 °C the Te products were a mixture of nanoparticles and tripod superstructures of various sizes. The planar tripod crystals became the dominant microstructures as the temperature was increased to above 120 °C. Each branch of the tripod crystal looks like a pine leaf. When the temperature was raised to 130 °C, the fascinating tripod Te superstructures became the dominant products.

At a still higher reaction temperature such as 140 °C, most of the tripod branches turned from pine leaf shape into rods with very rough surface. Further increase of the reaction temperature to 150 °C resulted in the products that consisted of mainly bulky materials and a small amount of Te tripod. When the reaction temperature was raised to 160 °C, there was almost no tripod shaped Te in the final products. These experiments confirm that the suitable reaction temperature for making planar tripod Te crystals is around 130 °C.A series of experiments with different compositions of $CHCl_3/C_2H_5OH$ solvent illustrate that the volume ratio of $CHCl_3/C_2H_5OH$ solution is also critical in determining the microstructure of the final products. When the volume ratio was increased to 1/1, the morphology of the Te superstructures turned into well-built tripod flake (see Figure S4 in the Supporting Information).

Figure 3 shows SEM, TEM, and HRTEM images and XRD analysis of the Au/Te hybrids. The low- and high-magnification

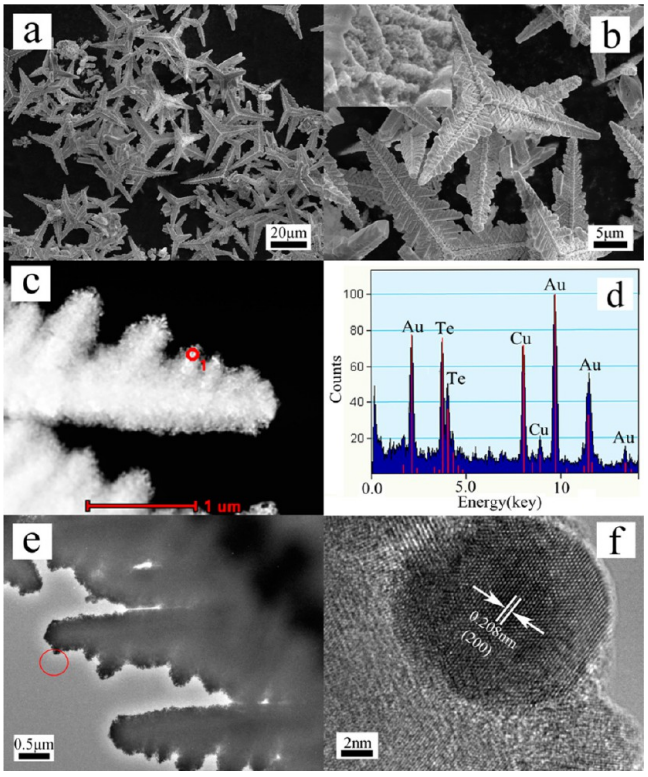

Figure 3. (a) Low-magnification SEM, (b) high-magnification SEM, (c) HADDF image, (d) EDX pattern, (e) TEM, and (f) HRTEM image of the Au-decorated Te hybrids. The circles in c and e indicate the area where the EDX spectra and HRTEM image were taken.

SEM images a and b in in Figure 3 illustrate that the tripod superstructure was not destroyed upon the coating of Au. Results in Figure 3c–e confirm the formation of Au-decorated Te superstructure. Notably, the Au/Te hybrids have a very rough surface, which is made up by many Au nanoparticles. Such a feature certainly provides a larger surface area for applications in catalysis etc. As illustrated by the HRTEM image in Figure 3f, Au crystals grew along (200) direction. The element distribution along a cross-section of a rod is also indicative of the formation of the hybrid structure (see Figure S5 in the Supporting Information).

The detection of arsenic using SWASV technique involves two steps: (i) The deposition of As(0) at an optimized potential for a certain period of time, and (ii) anodic stripping of the deposited As(0). In this study, the deposition time and applied potential were optimized to be 120 s and −0.3 V. In general, using a large negative potential would increase the magnitude of the subsequent anodic peak. From the perspective of low energy cost, −0.3 V was used here, except for the simultaneous determination of multiple heavy metal ions. The deposition time (120 s) was used to avoid the saturation response at higher concentrations of arsenic. Figure 4 shows the SWASV of As(III)

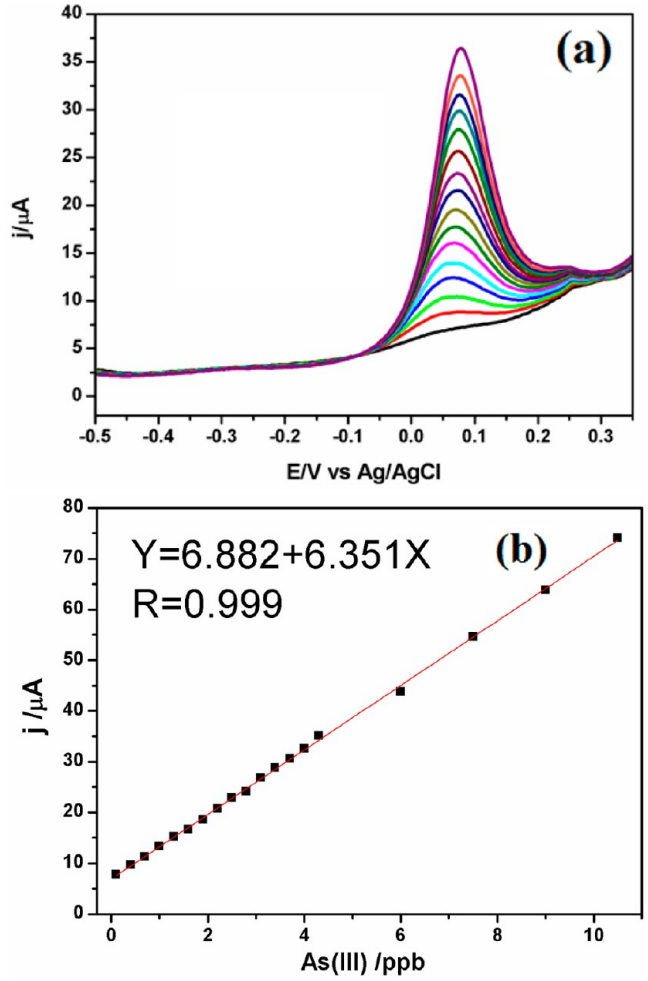

Figure 4. (a) Square wave anodic stripping current obtained at a Au/Te modified GC electrode in electrolyte solution containing 1.0 M HCl and different amounts of As(III): 0 (bottom line), 0.1 ppb (second lowest spectrum), and 0.3 ppb increment thereafter; (b) a linear relationship between As(III) concentration and the peak current.

in a 1.0 M HCl solution at the Au/Te electrode. In Figure 4a, a well-developed anodic peak is observed at the potential of 0.07 V, which corresponds to the oxidation of As(0) to As(III). The amplitude of this stripping peak increases, whereas the peak potential shifts slightly toward a more positive value, with respect to increasing As(III) concentration in the sample solution. The peak potential shift is generally connected to influences of surface morphology on the charge transfer process. SWASV conducted at high As(III) concentration can be found in Figure S6 in the Supporting Information. Figure 4b illustrates that the peak current has a linear relationship with the arsenic concentration in the solution and the linear increase is observed up to the concentration of 10 ppb. The sensitivity of this modified electrode is calculated as 6.35 μA/ppb from the slope of the above linear plot

dx.doi.org/10.1021/am401205w | ACS Appl. Mater. Interfaces 2013, 5, 5733−5740

(I = 6.688 + 6.351[As(III)] with a linear regression coefficient 0.999). The low detection limit is 0.0026 ppb based on S/N = 3. Such a detection limit is well below the guideline value of As(III) in drinking water set by WHO, suggesting that this platform is sensitive enough for potential practical applications.

To demonstrate the advantages of the Au/Te hybrid electrode, similar measurements were performed with a commercial Au electrode with the same physical size (2 mm in diameter). The bare Au electrode was coated with a layer of nafion film in order to mimic the fact that Au/Te particles were adhered together and to the GC electrode by nafion. Figure 5 shows the anodic peaks at

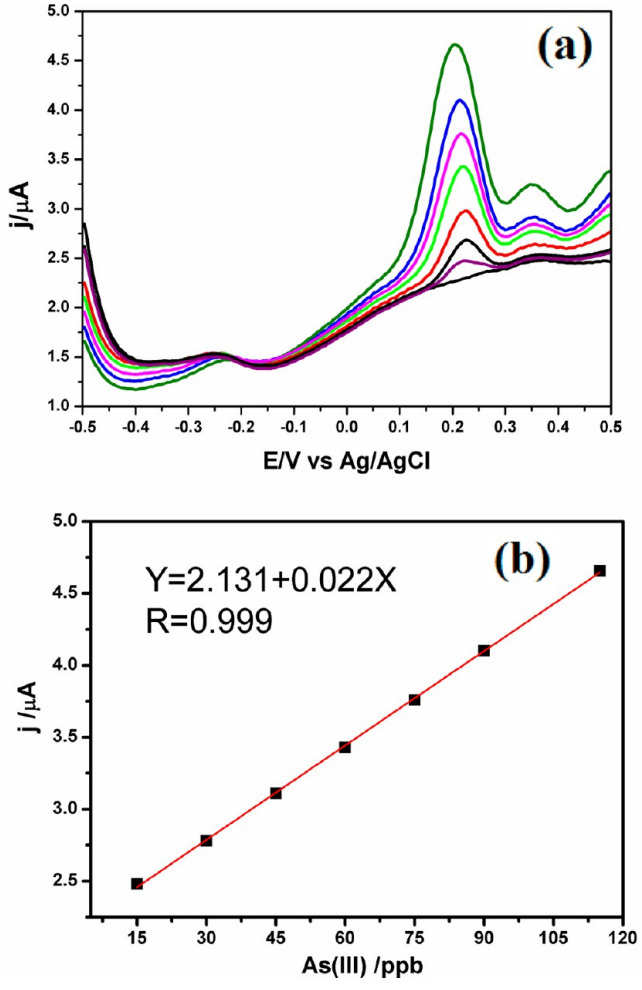

Figure 5. (a) Square wave anodic stripping current obtained at a bare Au electrode. The electrolyte consists of 1.0 M HCl and different amounts of As(III): 0, 15, 30, 45, 60, 75, 90, and 115 ppb (from bottom to top curve); (b) a calibration plot between the response current and the concentration of As(III).

different As (III) concentrations, while all other conditions are the same as those used in Figure 4. Here the anodic peak occurs at the potential of around 0.2 V, which is more positive than that seen at the Au/Te electrode. The current density also decreased significantly, where the linear fit in Figure 5b has a slope of 0.022 uA/ppb. The dramatic improvement in the electrocatalytic performance of Au/Te electrode shall be attributed to the increased kinks and ledges from the branched nanostructures, in addition to the increase in the surface to volume ratio. To further confirm that nafion did not contribute to the above observed improvement, nafion film was also casted on a GC electrode to detect 10 ppb As(III), there was no anoidic peak in the SWASV (see Figure S7 in the Supporting Information).

A challenge faced in the earlier electrochemical detection of As(III) with Au or Au nanoparticles is the interference from other heavy metal ions, in particular Cu(II), which has a redox potential of 0.339 V, very close to that of As(0). Figure 6a

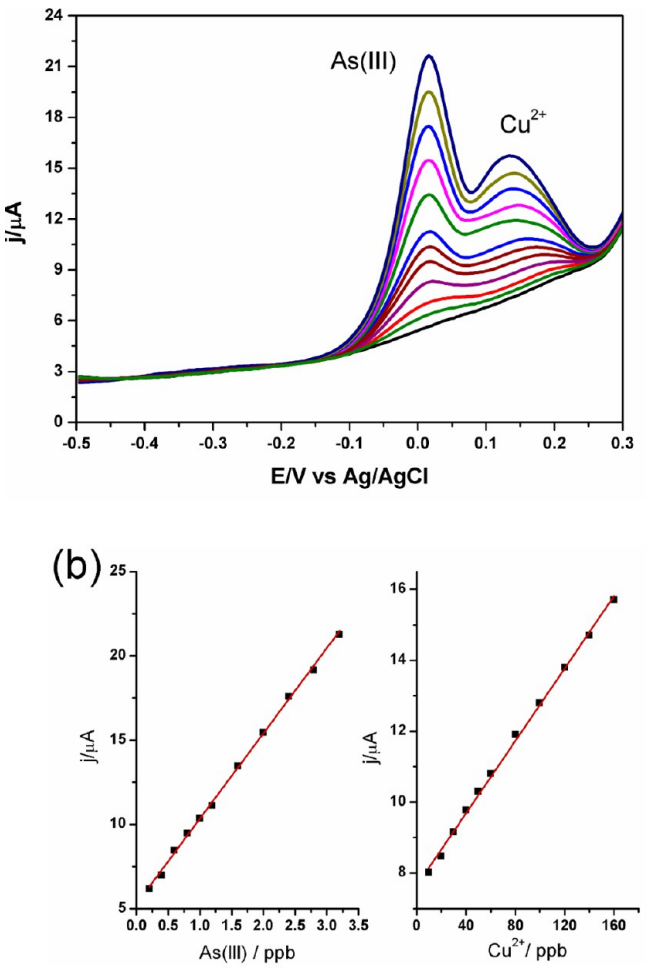

Figure 6. (a) Square wave anodic stripping current of As(III) and Cu(II) mixtures at the Au/Te modified GC electrode. The electrolyte consists of 1.0 M HCl and a mixture of As(III) and Cu(II): 0.2 and 10 ppb, 0.4 and 20 ppb, 0.6 and 30 ppb, 0.8 and 40 ppb, 1.0 and 50 ppb, 1.2 and 60 ppb, 1.6 and 80 ppb, 2.0 and 100 ppb, 2.4 and 120 ppb, 2.8 and 140 ppb, 3.2 and 160 ppb, respectively (from the bottom to top curve); (b) calibration plots of the response current versus the concentration of As(III) (I(μA) = 5.063 + 5.281[As(III)]) and versus copper concentration (I(μA) = 7.643 + 0.0517[Cu^{2+}]).

presents the anodic stripping peaks achieved in a mixture of As(III) and Cu(II), where an isolated anodic peak was obtained at about 0.16 V when Cu(II) became higher than 5 ppb. The peak potential is more than 100 mV away from the anodic peak of As(0). Here concentrations of As(III) and Cu(II) were increased simultaneously. In separate tests, when Cu(II) concentration was a sole variable to increase from 0 to 160 ppb, the peak current at 0.06 V only increased marginally, suggesting that the presence of Cu(II) in the solution had negligible influence on the detection of As(III) with this new Au/Te electrode. For comparison to the performance of other platforms developed for the electrochemical detection of As(III), Table 1 listed the data collected from literature. Those results illustrate that the Au/Te electrode

dx.doi.org/10.1021/am401205w | ACS Appl. Mater. Interfaces 2013, 5, 5733−5740

prepared in this research has the highest sensitivity, in addition to exhibiting a low detection limit.

Under the conditions used in this research, responses of the above Au/Te-modified GC electrode to different heavy metal ions are presented in Figure 7 (corresponding LSVs are presented

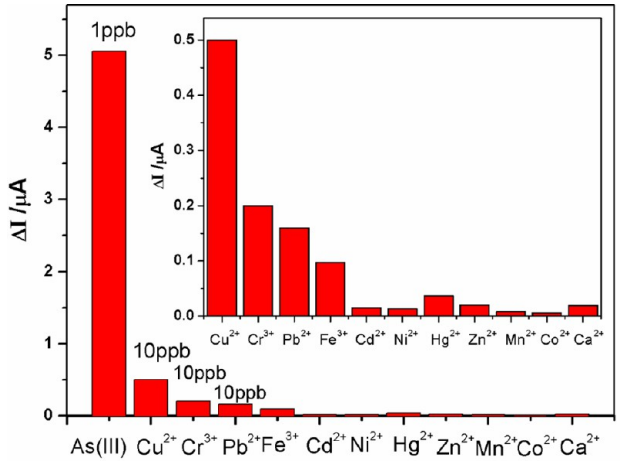

Figure 7. Response current of different metal ions at the Au/Te modified GC electrode. The concentration of As(III) is 1 ppb, whereas the concentration of all other ions tested here is 10 ppb.

in Figures S8 and S9 in the Supporting Information). Here the deposition took place at −0.3 V for 120 s. The great difference in the response current suggests that this new electrode has good selectivity in the detection of As(III). In this study we prepared 5 Au/Te electrodes each time and achieved good device-to-device reproducibility with a relative standard deviation (RSD) of less than 1.3%. After keeping the fabricated electrode in our lab for a month, the current intensity in the detection of arsenic decreases by less than 6.8%. However, the repeated usage of this hybrid electrode has irreversible influence on its performance, where the peak current decreases by about 25% after 100 continuous CV cycling. Such a change implicates that the 3D superstructure may have gradually collapsed, resulting in a decrease in the total number of active cites.

4. CONCLUSIONS

Tripod-shaped Au-decorated Tel crystallines are prepared in this study through a hydrothermal approach. Notably, this process does not require the assistance of any templates or surfactants. The 3D superstructure is conveniently manifested by controlling the ratio of $CHCl_3/C_2H_5OH$ solvent or the reaction temperature. The obtained Te superstructures are single crystalline in nature, in which both the main and secondary branches grow preferentially along the (100) direction. When the Au/Te hybrids modified GC electrode is employed to detect As(III) in water, the sensitivity is more than 2 orders better than that obtained with a bare Au electrode. The detection limit is about 0.0026 ppb with the Au/Te electrode. When an uncoated 3D Te was directly employed to detect As(III), the current response was poor (see Figure S10 in the Supporting Information). The great improvement in the electrochemical performance of Au/Te hybrids may be attributed to the unique 3D morphology, where the branched structure provides a large number of ledges and kicks for catalytic reactions and the planar structure of each rod further increases the surface area in comparison to regular tripod nanostructures.

■ ASSOCIATED CONTENT

Supporting Information

Characterizations of Te products including XRD, EDS, SEM, element distribution analysis, and additional square wave anodic stripping experiments. This material is available free of charge via the Internet at http://pubs.acs.org.

■ AUTHOR INFORMATION

Corresponding Author

*E-mail: shunwang@wzu.edu.cn (S.W.); jwang@uwindsor.ca (J.W.). Fax: 86-577-86683000 (S.W.); 1-519-973-7098 (J.W.).

Notes

The authors declare no competing financial interest.

■ ACKNOWLEDGMENTS

We are grateful for financial support from NSFC (21073133 and 51272182), Zhejiang Provincial Natural Science Foundation of China (Y4080177, Y4090248 and Y5100283), and Zhejiang Scientific and technological innovation fund (2012R424062 and 2012R424064).

■ REFERENCES

(1) Smedley, P. L; Kinniburgh, D. G. *Appl. Geochem.* **2002**, *17*, 517−568.
(2) Cullen, W. R.; Reimer, K. J. *Chem. Rev.* **1989**, *89*, 713−764.
(3) Mandal, B. K.; Suzuki, K. T. *Talanta* **2002**, *58*, 201−235.
(4) Nordstrom, D. K. *Science* **2002**, *296*, 2143−2145.
(5) Cavicchioli, A.; La-Scalea, M. A.; Gutz, I. G. R. *Electroanalysis* **2004**, *16*, 697−711.
(6) Dai, X.; Nekrassova, O.; Hyde, M. E.; Compton, R. G. *Anal. Chem.* **2004**, *76*, 5924−5929.
(7) Rahman, M. R.; Okajima, T.; Ohsaka, T. *Anal. Chem.* **2010**, *82*, 9169−9176.
(8) Feeney, R.; Kounaves, S. P. *Anal. Chem.* **2000**, *72*, 2222−2228.
(9) Hossain, M. M.; Islam, M. M.; Ferdousi, S.; Okajima, T.; Ohsaka, T. *Electroanalysis* **2008**, *20*, 2435−2441.
(10) Simm, A. O.; Banks, C. E.; Compton, R. G. *Anal. Chem.* **2004**, *76*, 5051−5055.
(11) Song, Y.; Swain, G. M. *Anal. Chem.* **2007**, *79*, 2412−2420.
(12) Kumar Jena, B.; Retna Raj, C. *Anal. Chem.* **2008**, *80*, 4836−4844.
(13) Simm, A. O.; Banks, C. E.; Wilkins, S. J.; Karousos, N. G.; Davis, J.; Compton, R. G. *Anal. Bioanal. Chem.* **2005**, *381*, 979−985.
(14) Profumo, A.; Fagnoni, M.; Merli, D.; Quartarone, E.; Protti, S.; Dondi, D.; Albini, A. *Anal. Chem.* **2006**, *78*, 4194−4199.
(15) Salimi, A.; Hyde, M. E.; Banks, C. E.; Compton, R. G. *Analyst* **2004**, *129*, 9−14.
(16) Zen, J.-M.; Chen, P.-Y.; Kumar, A. S. *Anal. Chem.* **2003**, *75*, 6017−6022.
(17) Male, K. B.; Hrapovic, S.; Santini, J. M.; Luong, J. H. T. *Anal. Chem.* **2007**, *79*, 7831−7837.
(18) Salimi, A.; Mamkhezri, H.; Hallaj, R.; Soltanian, S. *Sens.Actuators, B: Chem* **2008**, *129*, 246−254.
(19) Gao, C.; Yu, X,Y.; Xiong, S,Q.; Liu, J, H.; Huang, X, J. *Anal. Chem.* **2013**, *85*, 2673−2680.
(20) Shen, J.; Li, J.; Chen, Y.; Zhang, Z. *J. Phys. Chem. C* **2009**, *113*, 9502−9508.
(21) Ma, Y. R.; Qi, L. M.; Ma, J. M.; Chang, H. M. *Cryst. Growth Des.* **2004**, *4*, 351−354.
(22) Wiley, B. J.; Chen, Y.; McLellan, J. M.; Xiong, Y.; Li, Z. Y.; Ginger, D.; Xia, Y. *Nano Lett.* **2007**, *7*, 1032−1036.
(23) Narayanan, R.; El-Sayed, M. A. *J. Am. Chem. Soc.* **2004**, *126*, 7194−7195.
(24) Zhang, J.; Sun, L. D.; Jiang, X. C.; Liao, C. S.; Yan, C. H. *Cryst. Growth Des.* **2004**, *4*, 309−313.
(25) Zhu, T.; Chen, X.; Cao, Y.; Zhao, X. *J. Phys. Chem. C* **2009**, *113*, 8085−8091.

(26) Guo, S. J.; Dong, S. J.; Wang, E. K. *J. Phys. Chem. C* **2010**, *114*, 4797−4802.
(27) Samal, A. K.; Pradeep, T. *J. Phys. Chem. C* **2010**, *114*, 5871−5878.
(28) Xi, G. C.; Liu, Y. K.; Wang, X. Q.; Liu, X. Y.; Peng, Y. Y.; Qian, Y. T. *Cryst. Growth Des.* **2006**, *6*, 2567−2570.
(29) Zuo, P. F.; Zhang, S. Y.; Jin, B. K.; Tian, Y. P.; Yang, J. X. *J. Phys. Chem. C* **2008**, *112*, 14825−14829.
(30) Zhu, Y. J.; Wang, W. W.; Qi, R. J.; Hu, X. L. *Angew. Chem., Int. Ed.* **2004**, *43*, 1410−1414.
(31) Mohanty, P.; Kang, T.; Kim, B.; Park, J. *J. Phys. Chem. B* **2006**, *110*, 791−795.
(32) Song, J. M.; Lin, Y. Z.; Zhan, Y. J.; Tian, Y. C.; Liu, G.; Yu, S. H. *Cryst. Growth Des.* **2008**, *8*, 1902−1908.
(33) Wang, Q.; Li, G. D.; Liu, Y. L.; Xu, S.; Wang, K. J.; Chen, J. S. *J. Phys. Chem. C* **2007**, *111*, 12926−12932.
(34) Zhang, B.; Hou, W. Y.; Ye, X. C.; Fu, S. Q.; Xie, Y. *Adv. Funct. Mater.* **2007**, *17*, 486−492.
(35) He, Z. B.; Yu, S. H. *J. Phys. Chem. B* **2005**, *109*, 22740−22745.
(36) Narayanaswamy, A.; Xu, H. F.; Pradhan, N.; Kim, M.; Peng, X. G. *J. Am. Chem. Soc.* **2006**, *128*, 10310−10319.
(37) Cho, S.; Jang, J. W.; Kim, J.; Lee, J. S.; Choi, W.; Lee, K. H. *Langmuir* **2011**, *27*, 10243−10250.
(38) Lan, X. Z.; Jiang, Y.; Liu, X. M.; Wang, W. J.; Wang, B. B.; Wu, D.; Liu, C.; Zhang, Y. G.; Zhong, H. H. *Cryst. Growth Des.* **2011**, *11*, 3837−3843.
(39) Huang, D. P.; Bai, X. T.; Zheng, L. Q. *J. Phys. Chem. C* **2011**, *115*, 14641−14647.
(40) Siciliano, T.; Filippo, E.; Genga, A.; Micocci, G.; Siciliano, M.; Tepore, A. *Sen. Actuat. B Chem.* **2009**, *142*, 185−190.
(41) Zhao, A. W.; Ye, C. H.; Meng, G. W.; Zhang, L. D.; Ajayan, P. M. *J. Mater. Res.* **2003**, *18*, 2318−2322.
(42) Lu, J.; Xie, Y.; Xu, F.; Zhu, L. *J. Mater. Chem.* **2002**, *12*, 2755−2761.
(43) Jin, H.; Wang, D. M.; Zhao, Y. W.; Zhou, H.; Wang, S.; Wang, J. *J. Power Sources* **2012**, *215*, 227−232.
(44) Zhao, Y. W.; Jin, H. L.; Zhou, H.; Lin, J. J.; Wang, S.; Wang, J. *J. Phys. Chem. C* **2012**, *116*, 7416−7420.
(45) Gautama, Ujjal, K.; Rao, C. N. R. *J. Mater. Chem.* **2004**, *14*, 2530−2535.
(46) Liu, Z. P.; Hu, Z. K.; Liang, J. B.; Li, S.; Yang, Y.; Peng, S.; Qian, Y. T. *Langmuir* **2004**, *20*, 214−218.
(47) Wang, S.; Guan, W. P.; Ma, D. K.; Chen, X. A.; Wan, L.; Huang, S. M.; Wang, J. C. *CrystEngComm* **2010**, *12*, 166−171.
(48) Wang, S.; Zhang, K. J.; Zhou, H.; Guan, W. P.; Ma, D. K.; Lin, J. J.; Zhang, L. J.; Huang, S. M.; Wang, J. C. *CrystEngComm* **2010**, *12*, 3852−3857.
(49) Zhuang, Z. B.; Peng, Q.; Li, Y. D. *Chem. Soc. Rev.* **2011**, *40*, 5492−5515.